

Uterine scars after caesarean delivery: From histology to the molecular and ultrastructural level

Alexander Paping MD^{1,2}  | Clara Basler² | Loreen Ehrlich² | Carlo Fasting PhD³ | Kerstin Melchior² | Thomas Ziska² | Mario Thiele⁴ | Georg N. Duda PhD⁴ | Sara Timm PhD⁵ | Matthias Ochs MD, PhD^{5,6}  | Rebecca C. Rancourt PhD² | Wolfgang Henrich MD, PhD¹ | Thorsten Braun MD, PhD^{1,2} 

¹Department of Obstetrics, Charité – Universitätsmedizin Berlin, Corporate Member of Freie Universität Berlin and Humboldt-Universität zu Berlin, Berlin, Germany

²Division of Experimental Obstetrics, Charité – Universitätsmedizin Berlin, Corporate Member of Freie Universität Berlin and Humboldt-Universität zu Berlin, Berlin, Germany

³Institut für Chemie und Biochemie, Freie Universität Berlin, Berlin, Germany

⁴Julius Wolff Institute and Center for Musculoskeletal Surgery, Charité – Universitätsmedizin Berlin, corporate member of Freie Universität Berlin and Humboldt-Universität zu Berlin, Berlin, Germany

⁵Core Facility Electron Microscopy, Charité – Universitätsmedizin Berlin, Corporate Member of Freie Universität Berlin and Humboldt-Universität zu Berlin, Berlin, Germany

⁶Institute of Functional Anatomy, Charité – Universitätsmedizin Berlin, corporate member of Freie Universität Berlin and Humboldt-Universität zu Berlin, Berlin, Germany

Correspondence

Dr. med. Alexander Paping, Charité - Universitätsmedizin Berlin, Klinik für Geburtsmedizin, Campus Virchow-Klinikum, Augustenburger Platz 1, 13353 Berlin, Germany.
Email: alexander.paping@charite.de

Funding information

Deutsche Forschungsgemeinschaft Research Grants Program, Grant/Award Numbers: BR 2925/11-1, SCHW 1946/2-1; University Research Fund of Charité – Universitätsmedizin Berlin, Grant/Award Number: 51517172-01

Abstract

Uterine rupture during a trial of labor after caesarean delivery (CD) is a serious complication for mother and fetus. The lack of knowledge on histological features and molecular pathways of uterine wound healing has hindered research in this area from evolving over time. We analysed collagen content and turnover in uterine scars on a histological, molecular and ultrastructural level. Therefore, tissue samples from the lower uterine segment were obtained during CD from 16 pregnant women with at least one previous CD, from 16 pregnant women without previous CD, and from 16 non-pregnant premenopausal women after hysterectomy for a benign disease. Histomorphometrical collagen quantification showed, that the collagen content of the scar area in uterine wall specimens after previous CD was significantly higher than in the unscarred myometrium of the same women and the control groups. Quantitative real-time PCR of uterine scar tissue from FFPE samples delineated by laser microdissection yielded a significantly higher COL3A1 expression and a significantly lower COL1A2/COL3A1 ratio in scarred uteri than in samples from unscarred uteri.

Abbreviations: ATP5B, ATP synthase F1 subunit beta; CD, caesarean delivery; COL1A2, collagen type I alpha 2 chain; COL3A1, collagen type III alpha 1 chain; EIF2A, eukaryotic translation initiation factor 2A; group PS, group 'pregnant scarred uterus'; group PU, group 'pregnant unscarred uterus'; HPLC, high-performance liquid chromatography; IQR, interquartile range; LUS, lower uterine segment; ROI, region of interest; TEM, transmission electron microscopy.

This is an open access article under the terms of the [Creative Commons Attribution](#) License, which permits use, distribution and reproduction in any medium, provided the original work is properly cited.

© 2023 The Authors. *Wound Repair and Regeneration* published by Wiley Periodicals LLC on behalf of The Wound Healing Society.

Histological collagen content and the expression of COL1A2 and COL3A1 were positively correlated, while COL1A2/COL3A1 ratio was negatively correlated with the histological collagen content. Transmission electron microscopy revealed a destroyed myometrial ultrastructure in uterine scars with increased collagen density. We conclude that the high collagen content in uterine scars results from an ongoing overexpression of collagen I and III. This is a proof of concept to enable further analyses of specific factors that mediate uterine wound healing.

KEY WORDS

caesarean section, collagen, tissue remodelling, uterine rupture, uterine wound healing

1 | INTRODUCTION

Caesarean delivery (CD) leaves a scar in the uterus and constitutes the main risk factor for uterine rupture during subsequent delivery.¹ Until today, there are no drugs or techniques that enhance uterine wound healing at the time of CD to such an extent that the risk of uterine rupture during subsequent pregnancy could be eliminated.^{2,3} While scarring and fibrosis in the skin or the lung have been very intensively researched with stem cells-based organoid models and novel biological therapy approaches, scarring of the uterine wall is still a ‘neglected disease’ in the research area of tissue regeneration.^{4–7} One reason might stem from the fact that there exists no common histological definition of a uterine scar to date. Some publications have pointed out that uterine scars consist of more collagen than specimens from the unscarred uterine wall, but so far the amount of collagen in histological sections from uterine scars has not been quantified systematically.^{8–11} However, to compare wound healing of the uterus and to standardise analyzes of uterine scar tissue, a common definition of a uterine scar and quantifiable parameters of fibrosis of the uterine wall are needed. This is especially true when it comes to translating and comparing results from animal models to the human condition.^{12–14} Therefore, we sought to define the scarred region of the uterine wall histologically by quantifying the main characteristic of scars: their collagen content. As we believe that research on uterine scars will not evolve if we stay on the microscopic level by performing histology and immunohistology, we used laser-microdissection to perform RNA isolation, reverse transcription and, quantitative TaqMan real-time PCR analysis (qRT-PCR) from designated scar areas to test whether overexpression of collagen type I alpha 2 (COL1A2) and collagen type III alpha 1 (COL3A1) is the origin of histologically high collagen content. Collagen III is characterised by thinner fibril diameters and lowered mechanical strength than collagen I.^{15,16} We therefore calculated the COL1A2/COL3A1 ratio to test whether uterine scars exhibit a shift towards more collagen III which might explain a reduced mechanical strength of uterine scar tissue compared to unscarred myometrium.^{17,18} In comparison to these targeted investigations, we performed hydroxyproline measurements to quantify the collagen content in fresh frozen tissue without prior histological targeting as previously published by Buhimschi et al.¹⁰ Furthermore,

collagen cross-links were quantified based on the pyridinoline and deoxypyridinoline content of fresh frozen samples via high-performance liquid chromatography (HPLC).¹⁰ At last, the ultrastructure of scarred versus unscarred myometrium was evaluated qualitatively using transmission electron microscopy (TEM).

2 | MATERIALS AND METHODS

2.1 | Patient population

Women were recruited into three study groups: group PS ('pregnant scarred uterus'): pregnant women with at least one previous CD, group PU ('pregnant unscarred uterus'): pregnant women without previous CD and the control group: non-pregnant premenopausal women undergoing hysterectomy for a benign disease (uterus myomatous, hypermenorrhoea etc.). All women were healthy and older than 18 years of age. Enrollment took place prospectively at Charité—Universitätsklinikum in Berlin, Germany. Pregnant women were only enrolled in cases of singleton pregnancy. This study complied with all relevant national regulations, institutional policies and is in accordance with the tenets of the Helsinki Declaration (as revised in 2013) and has been approved by the authors' Institutional Review Board (Charité—Universitätsklinikum Berlin, Berlin, Germany; EA4/159/16). Informed consent was obtained from all individuals included in this study.

2.2 | Sampling

Sampling of uterine tissue from group PS and group PU was performed during elective (repeat) CD from the contraction-free uterus. After laparotomy, intraoperative ultrasound was performed to identify the thinnest part of the lower uterine segment, as previously described by us.¹⁹ Next, the uterine incision was performed 2 cm cranially to the thinnest part of the LUS (lower uterine segment) as the area of interest. Immediately after delivery of the infant and before administration of oxytocin and removal of the placenta, a sample of $\sim 0.5 \times 4.0 \text{ cm}^2$ was excised with a surgical scissor. To aid orientation of samples during further processing, a yellow dye was

applied to the serosal side of the sample and a green dye was applied to the side facing the uterotomy. Sampling of tissue from the control group was performed immediately after abdominal or laparoscopic hysterectomy. Control groups specimens were excised from a healthy area of the posterior LUS. All samples were divided into two parts: the first part was formalin fixed immediately and paraffin-embedded for further analyses. The second part was immediately frozen in liquid nitrogen and stored at -80°C . From samples of three women from group PS, a third part was prepared for TEM and processed as described below.

2.3 | Gomori trichrome staining to identify collagen fibres

Gomori trichrome Staining was performed as previously described.²⁰ Paraffin sections 5- μm thick were cut and dewaxed in xylene (2×5 min; J. T. Baker, Radnor, USA). Rehydration was carried out in ethanol (2 min each in 96%, 70%, 50%; Carl Roth, Karlsruhe, Germany) followed by incubation for 30 min at 56°C in Bouin solution. The sections were rinsed under running water for 5 min and incubated in Weigert's iron haematoxylin (Merck, Darmstadt, Germany) for 10 min followed by another rinsing under running water for 10 min. Afterwards, samples were incubated in trichrome solution (Sigma-Aldrich, Taufkirchen, Germany) for 25 min. Differentiation was done in 0.5% acetic acid (Merck, Darmstadt, Germany) for 2 min and 1 min followed by dehydration in ethanol (1 min 96%, 2 \times 2 min 100%) and xylene (2×5 min). The sections were then covered with Entellan® Neu (Merck, Darmstadt, Germany) and a cover glass. Due to staining, cytoplasm and erythrocytes are red, fibrin and muscle pink, nuclei blue to black, and collagen fibres green.

2.4 | Image acquisition and macro-based analysis

Images of the tissue sections were taken with digital microscopy systems Axioskop and Leica DM6 B and the high-resolution digital colour cameras AxioCam MRC 5 (Zeiss, Oberkochen, Germany) and Leica DFC9000 GT (Leica, Wetzlar, Germany). The samples were scanned at high magnification ($\times 50$) and processed in mosaic mode with the Axiovision 4.8.2 software (Zeiss, Oberkochen, Germany) or Leica Application Suite X (Leica, Wetzlar, Germany) to produce images of whole tissue sections. Afterwards, the area percentages of muscle tissue and collagen (the main component of scars²¹) were automatically calculated with a newly developed macro for the image processing software Fiji (NIH, Bethesda, USA), as previously described (Supporting Information 1 and 2).¹⁹ Three slides were examined per patient. The macro allows the user to draw a box-shaped region of interest (ROI) into the image of the tissue section. Subsequently, using thresholds for colour saturation or manual cutout, empty areas at the edge of the tissue or within a section were excluded from the analysis. Collagen areas around blood vessels were also excluded, as they constitute the adventitia and might distort the analysis. Then, the muscle and scar areas were dichotomized through thresholding of the hue, based on the Gomori trichrome

staining: muscle cells in pink and fibrous tissue in green. For group PS, the rectangular ROI was defined with the aim to contain as much of the collagen-rich scarred area of the specimen as possible and to extend beyond the transition area with decreasing content of fibrotic tissue to the unscarred myometrium. The ROI was subdivided into three sub-ROIs corresponding to the homogenous scar area, the unscarred myometrium and the transition area in the middle between scar and myometrium. This subdivision into three areas was based on our hypothesis that uterine ruptures may not necessarily occur exactly within uterine scars, but that possibly the transition area between muscle and scar represents the predetermined rupture site and should therefore be analysed separately. For group PU and the control group, the ROI was defined with the aim to contain a representative part of the sample, excluding the edges of the sample. Lastly, the areas occupied by scar tissue and muscle tissue in each (sub-)ROI were calculated automatically by the number of pixels and output as percentages.

2.5 | Laser microdissection and quantitative TaqMan real-time PCR analysis

RNA isolation from FFPE uterine scar tissue sections followed by RNA expression analyses in areas delineated by laser microdissection was carried out as previously published.²² Briefly, FFPE sample sections mounted on glass slides were stained with haematoxylin and eosin (HE). We stained a corresponding slide according to Gomori trichrome for orientation. Regions of interest in HE-stained samples were marked with laser microdissection (LMD) and subsequently scratched off the slide with a sterile scalpel. RNA extraction with RNeasy FFPE Kit (Qiagen, Hilden, Germany) and cDNA synthesis with iScript cDNA Synthesis Kit (BioRad, Feldkirchen, Germany) were carried out, and quantitative real-time PCR was performed on an ABI 7500 Real Time PCR System (Applied Biosystems, Life Technologies GmbH, Darmstadt, Germany). ATP synthase F1 subunit beta (ATP5B) and eukaryotic translation initiation factor 2A (EIF2A) were evaluated as reference genes. mRNA expression ATP5B was unaffected by respective study group conditions. Therefore, ATP5B was used for normalisation.²³ We used Applied Biosystems TaqMan primer assays (exon-spanning) (ID: COL1A2: Hs01028956 m1; COL3A1: Hs00943809 m1; ATP5B: Hs00969569 m1; EIF2A: Hs00230684 m1). Agarose gel (5%) electrophoresis was used to validate the amplified qRT-PCR products sizes and banding. Data are shown as ΔCq -values. COL1A2/COL3A1 ratio was calculated from respective ΔCq -values.

2.6 | Quantification of collagen: Hydroxyproline measurement

Hydroxyproline was measured in uterine tissue with a hydroxyproline assay (Cat. No. #MAK008, Sigma-Aldrich St. Louis, MO, USA) according to the manufacturer's protocol. 10 mg of fresh frozen uterine tissue was minced and lysed in 200 μL 6 M HCl solution for 4 h at 120°C and then cooled down. Hydrolysates were centrifuged, and the clarified supernatant was used for measurements. 10 μl of the 1 mg/mL hydroxyproline

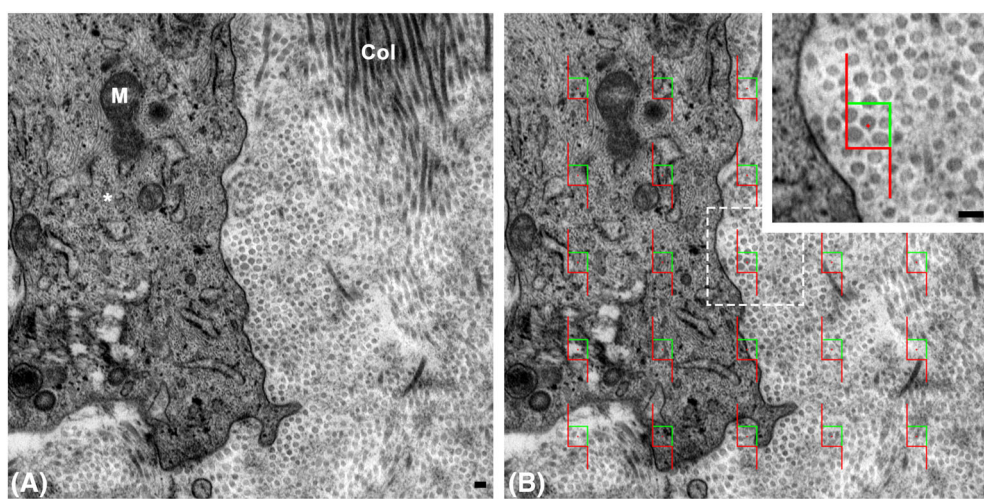


FIGURE 1 Quantitative ultrastructural collagen analysis. (A) Transmission electron microscopy image of an area determined by systematic uniform random area sampling with a fibroblast surrounded by collagen fibrils. (B) Same image as in A, overlaid with 25 counting frames. Inset shows an area for detailed evaluation. Cross-sectioned fibrils were included in the analysis if they appeared completely within the counting frame or touched the acceptance line (green) without touching the forbidden line (red). Scale bars = 100 nm. *, fibroblast; Col, collagen fibrils; M, mitochondrion.

standard solution was diluted in water to 0.1 mg/mL. Standards and the hydrolysate supernatant were pipetted in duplicates, transferred 2 µL to a 96-well plate and then dried on a heat plate at 60°C for 2 h. Afterwards, the assay reagents were prepared. 100 µL chloramine T/oxidation buffer mixture was added to all reaction wells. Incubation was performed at room temperature for 5 min. Colour development was achieved by incubation with 100 µL 4-dimethylaminobenzaldehyde/perchloric acid/isopropanol mixture at 60°C for 90 min. The absorbance was measured at 560 nm (Fluostar Omega, BMG Labtech GmbH, Ortenberg, Germany). All measurements were performed in a single assay to avoid inter-assay variability. The intra-assay variability was 8.6%. The total collagen concentration in the hydrolysate was calculated based on the assumption that collagen contains approximately 14% hydroxyproline.²⁴ Collagen concentrations were expressed in micrograms per milligram tissue.

2.7 | Quantification of collagen cross-linking, pyridinoline and deoxypyridinoline

Pyridinoline (PYD) and deoxypyridinoline (DPD) were quantified by ion pair chromatography on a RP-18 column, using perfluorobutyric acid (PFBt, HFbt) (Thermo Fisher Scientific, Waltham, MA, USA) as ion pair reagent, as previously published.^{10,25} Fresh frozen sample tissue (100 mg) was minced and lysed in 600 µL 10 N (32%) HCl solution for 20 h at 120°C. The cooled hydrolysates were centrifuged, and the clear supernatant was mixed with 2.6 mL washing solution B (acetone [Fisher Scientific, Schwerte, Germany]/acetic acid 4:1 v/v, w/o water). Crosslinks were isolated from the diluted hydrolysate by applying solid phase extraction on self-packed cellulose solid phase extraction (SPE) columns. These cellulose columns were prepared from 100 mg of cellulose powder (Sigma-Aldrich, St. Louis, MO, USA) and pre-fritted 6 mL SPE columns (Supelco, Bellefonte, PA, USA),

finally sealed with a second frit (Supelco). The columns were equilibrated with 5 mL washing solution A (acetonitrile/acetic acid/water 4:1:1 v/v) in parallel on a vacuum manifold (Machery-Nagel, Düren, Germany) with a vacuum of 800 mbar. The diluted hydrolysate solution was transferred onto the SPE column and allowed to soak in with the aid of a slight vacuum. Afterwards, the column was washed four times each with 5 mL of washing solution A and the eluates were discarded. Finally, the absorbed crosslinks were eluted by purging the SPE column five times each with 1 mL of distilled water and collecting the eluates in a single 20 mL falcon tube. The final eluate was lyophilized to dryness and stored at -20°C until HPLC measurement. For HPLC measurements, the lyophilizate was resuspended in 15% MeCN/15 mM perfluorobutyric acid (PFBt) and applied to a Waters Nova-Pak C18 column (4 µm, 150 × 3.9 mm², Waters Corp., Milford, MA, USA), with 15% MeCN/15 mM PFBt as mobile phase in isocratic measurement at 21°C with a flow rate of 1.5 mL·min⁻¹. A Smartline HPLC system (Knauer, Berlin, Germany), equipped with an autosampler and a RF-20A fluorescence detector (Shimadzu, Berlin, Germany) was employed. Pyridinoline and deoxypyridinoline were identified and quantified by their autofluorescence at 297 nm excitation and 395 nm emission based on comparison with an external calibration standard (Quidel, Athens, OH, USA). The fluorescence sensitivity magnification was set to 4096. The calibration range was between 1.5 and 76 fmol (PYD) and 0.7–37 fmol (DPD) per injection (5 µL each).

2.8 | Transmission electron microscopy

From three patients, tissue samples were fixed with 2% paraformaldehyde (Electron Microscopy Sciences, Hatfield, United States) and 2.5% glutaraldehyde (Serva, Heidelberg, Germany) in 0.1 M sodium cacodylate buffer (Serva, Heidelberg, Germany) for 30 min at RT and stored at 4°C. The samples were postfixed with 1% osmium tetroxide

TABLE 1 Demographic data of the study population.

Variable	Group PS (<i>n</i> = 16)	Group PU (<i>n</i> = 16)	Control group (<i>n</i> = 16)	<i>p</i> value
Maternal age (years) ^a	36 (30–38)	36 (27–38)	44 (39–50)	<0.001
BMI ^a	27 (20–36)	27 (22–32)	26 (23–30)	0.85
Gravidity ^b	4 (3–5)	2 (1–3)	n/a	<0.01
Parity ^b	2 (1–3)	1 (0–2)	n/a	0.02
Number of previous CD ^b	1 (1–3)	0	n/a	<0.001
Years since last delivery ^{b,c}	4 (2–5)	5 (3–11)	n/a	0.15
Gestational age at CD (weeks) ^b	39 (39–39)	39 (39–40)	n/a	0.88

Note: Statistically significant *p*-values (<0.05) are marked as bold text.

Abbreviations: BMI, body mass index; CD, caesarean delivery.

^aData presented as median (IQR) and analysed with Kruskal–Wallis test.

^bData presented as median (IQR) and analysed with Mann–Whitney *U* test.

^cGroup PS: years since last caesarean delivery, group PU: years since last vaginal delivery (*n* = 8 patients in group PU with at least one previous delivery).

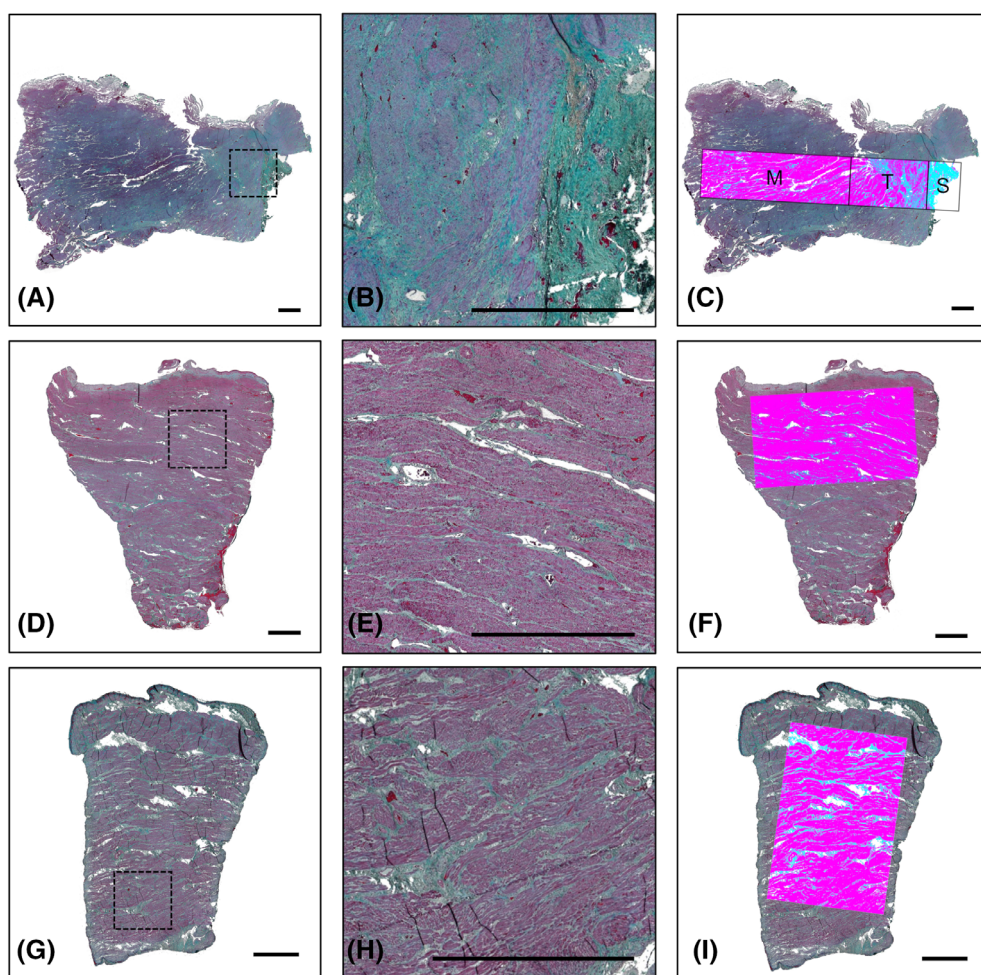


FIGURE 2 Histomorphology of uterine scars and unscarred myometrium. Samples from group PS (A–C), group PU (D–F), and the control group (G–I). Histological sections of the harvested tissue stained according to Gomori Trichrome. Staining shows muscle cells in pink and collagen fibres in green. (A) Uterine wall specimen from group PS. (B) Magnification of the scarred area outlined in (A). (C) Region of interest (ROI) as defined in the software program Fiji. Muscle tissue is shown in pink and scarred tissue in blue. The sub-ROI corresponding to the scarred area is denoted as 'S', the area of unscarred myometrium is denoted as 'M' and the transition area in between as 'T'. (D) Histological section of a tissue specimen from group PU. (E) Magnification of the area outlined in (D). (F) Region of interest (ROI) as defined in the software program Fiji. As no scar tissue is present, only a single ROI containing most parts of the sample was analysed. (G) Histological section of a tissue specimen from the control group. (H) Magnification of the area outlined in (G). (I) Region of interest (ROI) as defined in the software program Fiji. As no scar tissue is present, only a single ROI containing most parts of the sample was analysed. Sample surface facing the outer (serosal) oriented upwards and the surface facing the inner (endometrial) side is oriented downwards. Scale bars = 2 mm.

(Electron Microscopy Sciences, Hatfield, USA) and 0.8% potassium ferrocyanide II (Roth, Karlsruhe, Germany) in 0.1 M cacodylate buffer. After dehydration in a graded ethanol series the samples were transferred to Epon resin (Roth, Karlsruhe, Germany). Finally from the hardened tissue blocks, ultrathin sections (70 nm) were prepared using an ultramicrotome (Leica, Wetzlar, Germany) and a diamond knife (Diatome, Nidau, Switzerland), collected on pioloform-coated copper grids (Plano, Wetzlar, Germany) and stained with lead citrate (Merck Millipore, Darmstadt, Germany) according to Reynolds.²⁶ Grids were examined with a Zeiss Leo 906 electron microscope (Carl Zeiss, Oberkochen, Germany) at 80 kV acceleration voltage equipped with a slow scan 2 K CCD camera (TRS, Moorenweis, Germany). For quantitative analyses, investigators were blinded. The images were taken using a systematic uniform random sampling protocol at a primary magnification of $\times 21.560$.²⁷ The numerical density of cross-sectioned collagen fibrils was stereologically evaluated with an unbiased counting frame.²⁸ In addition, the diameter of collagen fibrils was measured simultaneously. The open source software ImageJ (Version 1.52, NIH, Bethesda, USA) and the counting frame macro (https://imagej.nih.gov/ij/macros/Unbiased_Frames.txt) were used. Twenty five counting frames were analysed per image (Figure 1). A cross-sectioned fibril was only included in the analysis if it was completely within the counting frame or if it touched the acceptance line without touching the forbidden line (Figure 1B inset). Not clearly identifiable fibrils due to orientation or overlap within the section, were not included in the analysis. Collagen density and fibril diameter in scarred and unscarred myometrium were compared. A minimum of 100 counting events was evaluated in each sample. The fibril density was defined as the sum of all counted fibrils in each sample per total counting frame area.

2.9 | Statistical analysis

Sample size calculation was performed with the software nQuery + nTerim 3.0.²⁹ Due to the lack of publications quantifying molecular biological aspects of uterine wound healing, the calculation is based on a clinical ultrasound paper by Sevket et al.³⁰ In this study, 36 women were randomised into two groups and underwent closure of the uterotomy by single-layer or double-layer suture during elective caesarean section. The primary outcome measure is the thickness of the lower uterine segment in mm on transvaginal ultrasound (hydrosonography) 6 months after CD.³⁰ Analysis of variance showed that to detect differences between three groups, 16 samples per group would be needed ($\alpha = 0.05$, power = 0.80). Data were tested for normality assessing the histogram. Comparisons between groups were performed using Mann–Whitney U test and Kruskal–Wallis test for independent samples and Wilcoxon signed-rank test and Friedman's ANOVA for matched samples. Data are reported as median and interquartile range (IQR). SPSS Version 28 (IBM, Chicago, USA) and GenEx Professional Software (Thermo Fisher Scientific, Waltham, MA, USA) were used for statistical analyses. Figures were prepared with Prism 8 (GraphPad Software, San Diego, USA). In all analyses, two-tailed $p \leq 0.05$ were considered to indicate statistical significance. Multiple comparisons were executed stepwise step-down.

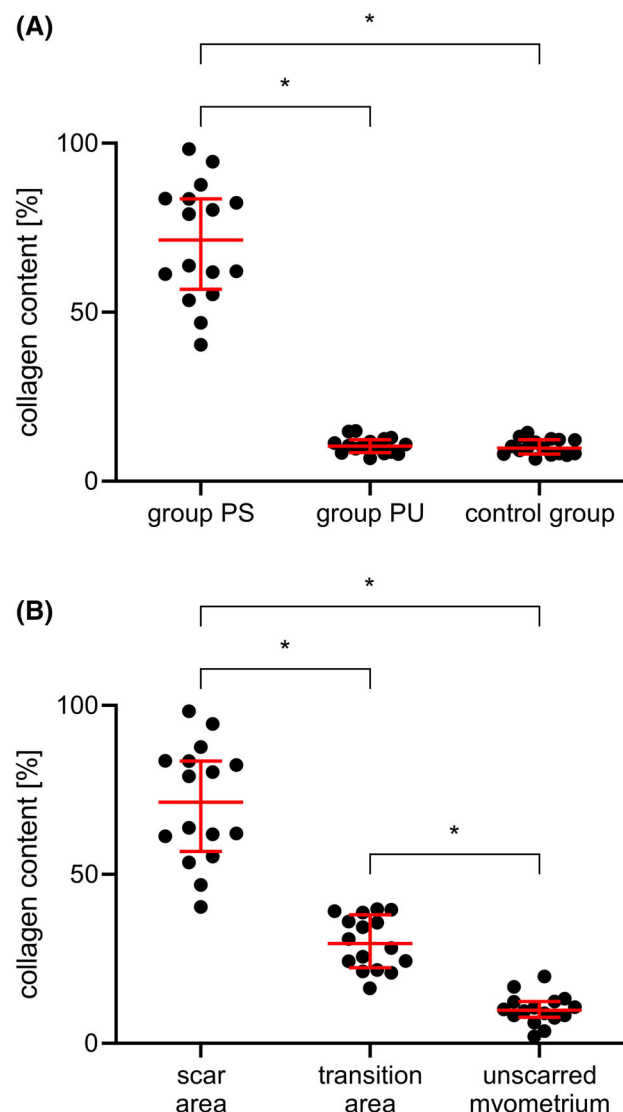


FIGURE 3 Histological collagen content in myometrial samples from the three study groups ($n = 48$). (A) Collagen content in the scar area of group PS contained significantly more collagen than samples from group PU and the control group ($p < 0.05$). Group PU and the control group showed similar amounts of collagen ($p = 0.46$). (B) For group PS, three regions were evaluated separately (scar region, transition region, unscarred myometrium). All regions differed significantly in terms of collagen content ($p < 0.001$). Histological collagen content in Gomori Trichrome-stained samples was determined with the software Fiji (NIH, Bethesda, USA). *, p value <0.05 ; ns, not significant.

3 | RESULTS

3.1 | Clinical characteristics of women

Demographic data of included women in the three groups is shown in Table 1. Women in the control group were significantly older than women in groups PS and PU ($p < 0.001$), however, there was no significant difference between patient ages of group PS and group PU

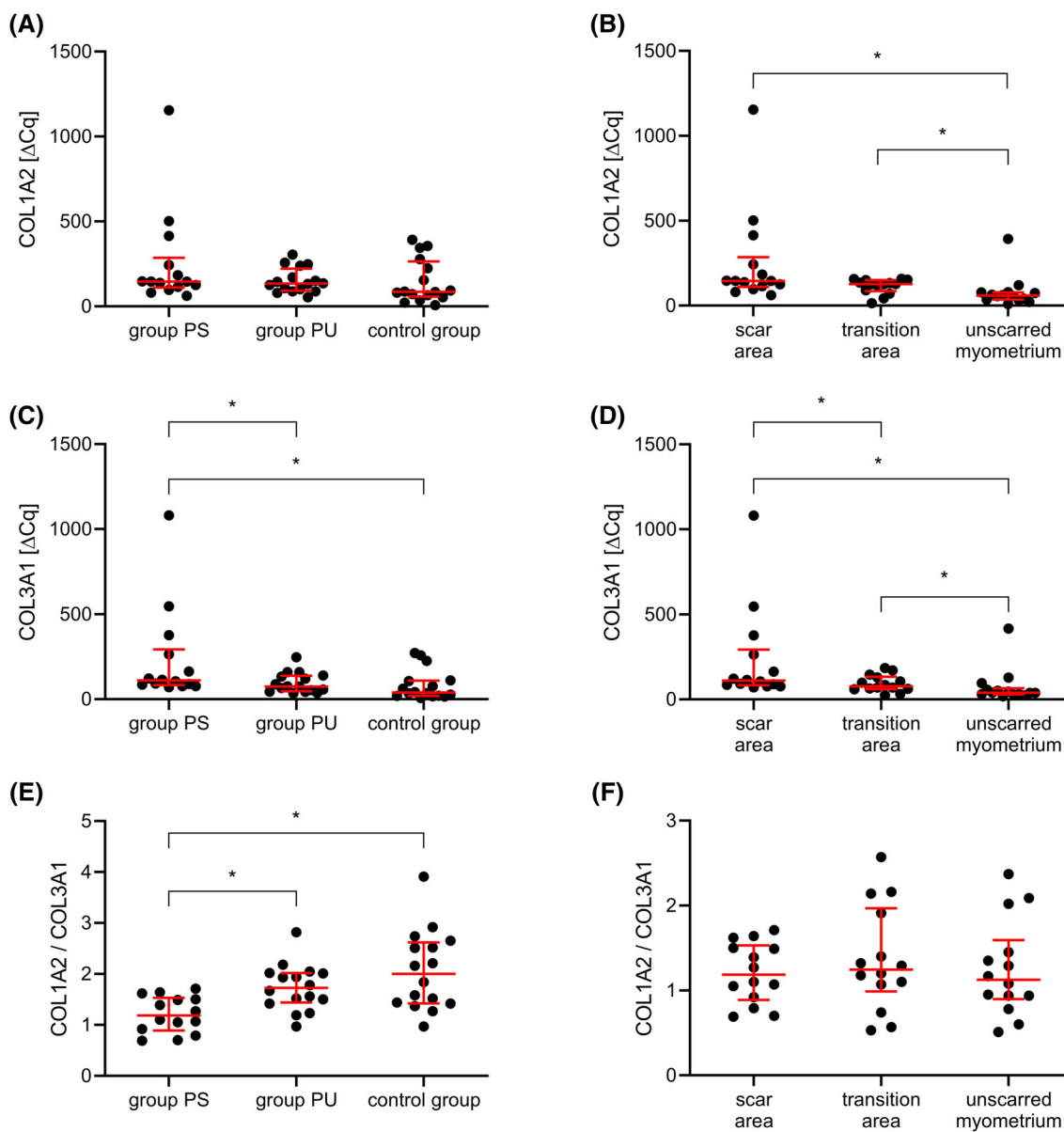


FIGURE 4 Gene expression of collagen type I alpha 2 (COL1A2) and collagen type III alpha 1 (COL3A1) in myometrial samples. Relative gene expression of COL1A2 and COL3A1 normalised to reference gene ATP5B. (A) COL1A2 ΔCq -values for group PS (scar area, $n = 14$), group PU ($n = 16$) and control group ($n = 16$) ($p = 0.22$). (B) COL1A2 ΔCq -values from group PS for scar area, transition area and unscarred myometrium (group PS, $n = 14$) ($p < 0.01$). (C) COL1A2 ΔCq -values for group PS (scar area, $n = 14$), group PU ($n = 16$) and control group ($n = 16$) ($p < 0.01$). (D) COL3A1 ΔCq -values from group PS for scar area, transition area and unscarred myometrium (group PS, $n = 14$) ($p < 0.001$). (E) COL1A2 / COL3A1 ratio (ΔCq -values) for group PS (scar area, $n = 14$), group PU ($n = 16$) and control group ($n = 16$) ($p = 0.02$). (F) COL1A2 / COL3A1 ratio (Cq -values) from group PS for scar area, transition area and unscarred myometrium (group PS, $n = 14$) ($p = 0.75$). * p value <0.05 ; ns, not significant.

($p = 0.97$). Gravidity and parity were slightly higher in group PS than in group PU ($p < 0.01$, $p = 0.02$).

3.2 | Histological scar tissue assessment and collagen content measurements

As previously described, we found that only some myometrial samples taken from women after previous CD (group PS) contained a

region with a high share of collagen.¹⁹ This region constituted only a part of the total sample and was identified as uterine scar tissue, defined by a collagen content of more than 40% (Figure 2A-C). Altogether, 53 samples were harvested for group PS, of which only 16 showed a histological positive detection of scar tissue. The other 37 samples with histological negative detection of scar tissue were not included in the study. Samples from groups PU and the control group contained a homogenous distribution of myometrial cells with little collagen in between. In these samples, no

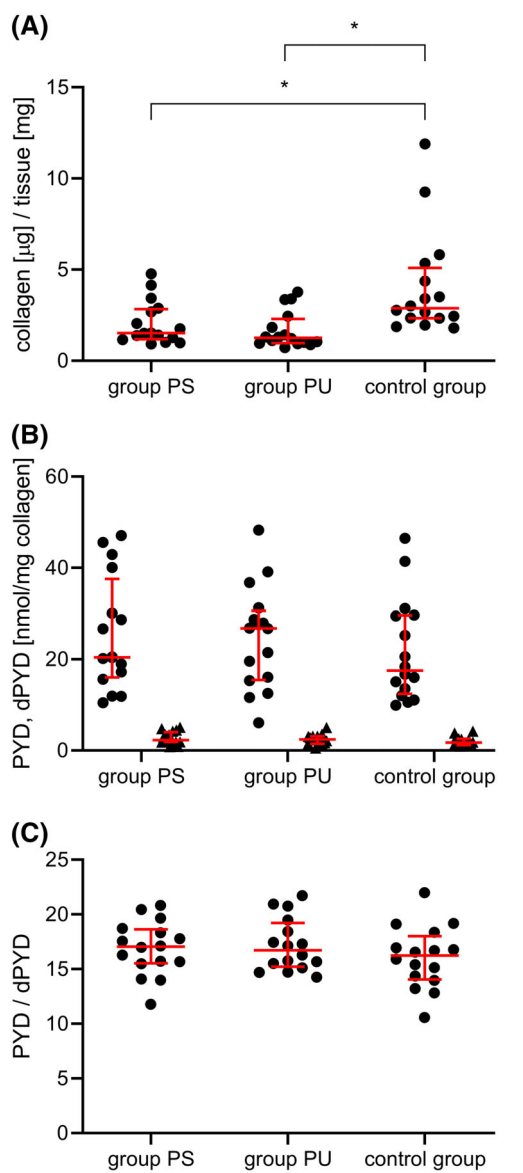


FIGURE 5 Quantification of collagen and collagen cross-linking ($n = 48$). (A) Quantification of collagen by hydroxyproline measurement in $\mu\text{g}/\text{mg}$ tissue ($p < 0.001$). (B) Pyridinoline and deoxypyridinoline content in myometrium specimens relative to the total amount of collagen as estimated from hydroxyproline measurements (PYD: $p = 0.58$, dPYD: $p = 0.31$). (C) Pyridinoline/deoxypyridinoline ratio in biopsies from the lower uterine segment ($p = 0.46$). Data are shown as median \pm interquartile range. *, $p < 0.05$; ns, not significant; PYD, pyridinoline; dPYD, deoxypyridinoline.

regionally differentiated distribution of collagen could be identified (Figure 2D–I). Samples from group PU and the control group contained significantly less collagen than the scar area in samples from group PS (group PS: 71.4% [56.8–83.6], group PU: 10.4% [8.5–12.3], control group: 9.8% [8.1–12.3], $p < 0.001$) (Figure 3A). Within group PS, collagen content of the scar area in uterine wall specimens was significantly higher than in the transition area [29.6% [23.7–36.8]] and the unscarred myometrium [9.8% [8.1–

12.6]] ($p < 0.001$) (Figure 3B). The collagen content in the unscarred myometrium of group PS was 9.8% (8.1–12.6) and was not significantly different from the collagen contents in group PU and the control group ($p = 0.75$). No outliers were excluded to reflect the heterogeneity of uterine wall fibrosis. The inter-assay coefficient of variation was 14.8%.

3.3 | Laser microdissection and quantitative TaqMan real-time PCR analysis

COL1A2 and COL3A1 expression analyses were successful in all samples except two samples from group PS due to limited sample material ($n = 74$). There was no significant difference in the overall expression of COL1A2 between the three study groups (Figure 4A, $p = 0.22$). Within group PS, COL1A2 was significantly higher expressed in the scar area and the transition area compared to the unscarred myometrium (Figure 4B, $p < 0.01$). COL3A1 expression was significantly higher in group PS than in group PU and the control group (Figure 4C, $p < 0.01$). Within group PS, COL3A1 was significantly higher expressed in the scar area compared to the transition area and lowest in the unscarred myometrium (Figure 4D, $p < 0.001$). COL1A2/COL3A1 ratio was significantly lower in the scar area of group PS compared to group PU and the control group (Figure 4E, $p = 0.02$). There was no significant difference in the COL1A2/COL3A1 ratio between the three areas of interest in samples from group PS (Figure 4F, $p = 0.75$). Overall, histological collagen content [in %] was positively correlated with expression of COL1A2 ($r = 0.33$, $p < 0.01$) and COL3A1 ($r = 0.4$, $p < 0.001$). COL1A2/COL3A1 ratio was negatively correlated with the histological collagen content ($r = -0.27$, $p = 0.03$). No outliers were excluded to reflect the heterogeneity of uterine wall fibrosis.

3.4 | Quantification of collagen by hydroxyproline measurement

The myometrium from fresh frozen tissue of non-pregnant women without prior histological targeting had a collagen content of 2.9 (1–5) $\mu\text{g}/\text{mg}$ tissue. This was significantly higher compared to myometrium from pregnant women with a scarred LUS 1.5 (1, 2, 8) $\mu\text{g}/\text{mg}$, and with a non-scarred LUS: 1.3 (1.0–2.3) $\mu\text{g}/\text{mg}$ (Figure 5A).

3.5 | Quantification of collagen cross-linking

In fresh frozen tissue without prior histological targeting, the myometrial pyridinoline content was 10 times higher than the deoxypyridinoline content in the three study groups (Figure 5B). Samples from all three groups showed a similar degree of cross-linking of the fibrillary collagen as represented by their PYD/dPYD ratio (group PS: 15.5 [13.3–17.0] nmol/mg, group PU: 15.2 [14.6–16.7] nmol/mg, control group: 14.1 [12.1–16.2] nmol/mg) (Figure 5C).

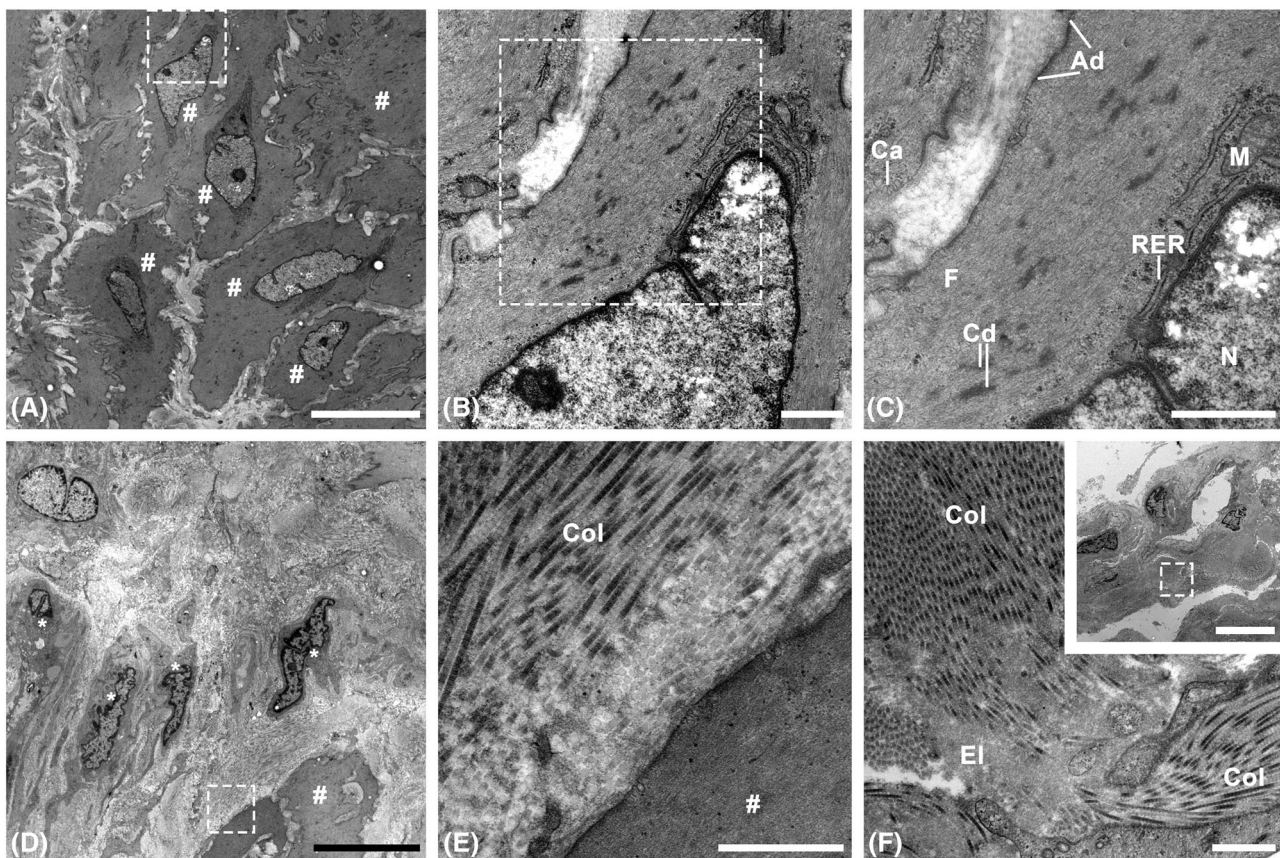


FIGURE 6 Ultrastructure of unscarred (A–C) and scarred myometrium (D–F) visualised by transmission electron microscopy. (A) Overview of smooth muscle cells. (B, C) Higher magnification of boxed areas indicated in A and B. The smooth muscle cells show a characteristic ultrastructure with numerous myofilaments, dense oval bodies ('corpuscula densa'), attachment plaques ('areae densae'), caveolae and cell organelles like rough endoplasmic reticulum and mitochondria next to the cell nucleus. (D) Overview of scar area with fibroblasts and few smooth muscle cells surrounded by ground substance. Boxed area indicated in D is shown in higher magnification in E. (E, F) Higher magnifications showing extracellular matrix consisting of collagen fibrils, elastic fibres and unformed ground substance. Collagen fibrils appear more frequently. Inset with boxed area in F shows the corresponding overview. Scale bars: A, D and inset in F = 10 µm; B, C, E, F = 1 µm. #, smooth muscle cell; *, fibroblast; Ad, areae densae; Ca, caveolae; M, mitochondrion; N, cell nucleus; RER, rough endoplasmatic reticulum; F, myofilaments; Cd, corpuscula densa; Col, collagen fibrils; El, elastic fibres.

3.6 | Ultrastructure of scarred versus unscarred myometrium

Transmission electron microscopy (TEM) revealed the altered ultrastructure of scarred myometrial samples. Unscarred areas (Figure 6A–C) show a regular myometrial architecture with one myometrial cell next to the other. Individual cells are surrounded by a thin basal lamina (Figure 6A). The cells exhibit the typical characteristics like elongated cell nuclei in the middle of the cell. Ultrastructurally, nearly lengthwise oriented myofilaments, numerous small densities in the cytoplasm (dense bodies: corpuscula densa) and on the plasma membrane (dense plaques: areae densae) can be seen. Numerous caveolae are present. The cell organelles such as rough ER and mitochondria are located near the nucleus (Figure 6B,C). In scar areas, this ordered structure is destroyed and replaced by large areas with extracellular matrix deposition (collagen fibrils, elastic fibres and unformed ground substance), with collagen fibrils predominating. Smooth muscle cells are sparsely represented, whereas fibroblasts can be seen

(Figure 6D–F). Median fibril density was 482 fibrils/µm² (exact values from three patients: 380, 482, 578 fibrils/µm²) in the scar area and 138 fibrils/µm² (exact values from three patients: 92, 138, 183 fibrils/µm²) in the unscarred myometrium ($p = 0.11$). Median fibril diameter was 52.1 nm (exact values 49.0, 52.1, 53.1 nm) in the scar area and 51.6 nm (exact values: 48.2, 51.6, 55.4 nm) in the unscarred myometrium ($p = 0.59$).

4 | DISCUSSION

The study has shown the accuracy of histologically-guided examination of uterine scars. The histologically assessed amount of collagen is significantly higher in uterine scars than in unscarred myometrium of both pregnant and non-pregnant uteri with a histological area percentage of >40% collagen in uterine scar tissue, 20%–40% in the transition area and <20% in unscarred myometrium. Uterine scars showed an increased COL1A2 and COL3A1 expression compared to

unscarred myometrium from the same patients. COL3A1 expression was higher and the COL1A2/COL3A1 ratio was significantly lower in scarred uteri than in samples from women with unscarred uteri. Overall, there were significant positive correlations between histological collagen content [in %] and expression of COL1A2 and COL3A1. COL1A2/COL3A1 ratio was negatively correlated with the histological collagen content. Examinations without histologically guided choice of the ROI, such as hydroxyproline measurements and quantification of collagen cross-linking of frozen myometrial samples were not able to show differences between the groups PS and PU. Interestingly, hydroxyproline measurements in fresh frozen tissue without prior histological targeting did not show a difference in scarred versus unscarred myometrium from pregnant women but indicated a higher collagen content in samples from the non-pregnant control group. The results suggest that neither the time since the last delivery nor whether a patient had previously carried a child to term has significantly skewed the data presented. Transmission electron microscopy revealed a destroyed myometrial ultrastructure in uterine scars with large areas of extracellular matrix deposition (collagen fibrils, elastic fibres and unformed ground substance), with collagen fibrils predominating. The number of smooth muscle cells was reduced while more fibroblasts were seen. Collagen density was more than three times higher in scarred myometrium compared to unscarred myometrium. Thus, the qualitative impression of a higher collagen content in the scarred area, in comparison to the unscarred area, could also be reproduced quantitatively. The simultaneous determination of the fibril diameter did not reveal any significant difference between unscarred and scarred areas. In this study, 37 out of 53 samples taken from the LUS of women with previous CD (group PS) did not show a uterine scar and examinations without histologically guided choice of the ROI did not yield results comparable to the differences between the three study groups detected by histomorphometry and confirmed by qRT-PCR. Accordingly, a publication that investigated the collagen content of specimens from the LUS of 68 women with or without previous CD yielded inconclusive results.¹⁰ Wu et al. did not find different amounts of collagen after immunohistochemical staining of the lower uterine segment in groups of women with and without prior CD.⁹ Both studies do not report an exact histological identification of the uterine scar before performing downstream analyses. We believe that these results might reflect that the examined tissue samples of women with prior CD did not contain the full amount of scar tissue. As FFPE-samples from group PS contained varying amounts of scar tissue, laser microdissection enabled effective sampling of ROIs for downstream quantitative PCR. Without this targeted approach, the samples contain too much unscarred myometrium. It appears plausible that this could be the reason for the inconclusive results of the hydroxyproline measurements and the collagen cross-linking quantification from fresh frozen tissue performed in this study without prior histological targeting. Besides the quantification of collagen fibres as a major component of uterine scars, this study has revealed the ongoing upregulation of collagen I and III formation by uterine fibroblasts. While previous histological descriptions of uterine scars might evoke the idea that the process of wound healing after a

previous CD has resulted in a persisting scar, the upregulation of intra-cellular COL1A2 and COL3A1 mRNA as shown with qRT-PCR proves the enhanced collagen synthesis at the time of sampling after previous CD. This aspect is in line with findings on tissue fibrosis of the liver, lung or skin. Collagen is continuously produced and degraded. To prevent organ fibrosis, the body needs to keep production and degradation in balance.³¹ Especially injury can activate collagen remodelling pathways that influence tissue integrity in fibrotic areas.³¹ Vascular collagen, for example, has a normal half-life of 60–70 days,³² which decreases by up to 10-fold in the case of disease and injury.³³ We postulate that the growth of the uterus and the mechanical stress generated in a uterine scar during pregnancy might induce increased collagen remodelling. As seen in this study, collagen III expression is increased stronger than collagen I expression in uterine scars, which is also reflected in the decreased COL1A2/COL3A1 ratio. In general, collagen III is synthesised in the early stages of wound healing and is replaced by collagen I, leading to an increased tensile strength of the scar tissue.^{18,34} Increased collagen III production and reduced collagen I/collagen III ratio underlines the idea of an active scar remodelling during pregnancy that might eventually lead to more connective tissue elasticity but possibly less strong uterine scar tissue. This study is the first to move from descriptive assessments of microscopic images of uterine scars to the molecular level by correlating uterine scar histomorphometry to local collagen gene expression. Due to the risk of uterine scar rupture during birth after previous CD, obstetricians are increasingly recommending a repeat CD and pregnant women are hesitant to go for a trial of labor after previous CD. To date, no effective techniques to enhance uterine wound healing post-CD have been described. Only a few studies have attempted to describe uterine scarring. We hope that our approach will help uterine scarring research to evolve further over time with the aim of finding possible therapeutic approaches to enhance uterine wound healing so that more women can experience a safe trial of labor after CD without having to fear uterine rupture. This study has shown that laser microdissection enables effective sampling of ROIs for downstream quantitative PCR. Without this targeted approach, samples from the scarred LUS contain too much unscarred myometrium. We recommend LMD-guided sampling of uterine scar tissue for future studies on uterine scarring. Further research might evaluate the expression of other genes that code for growth factors, matrix metalloproteinases or other factors involved in wound healing and scar remodelling.^{28,35} These targets could also be evaluated in trials that test the effect of different uterotomy closure techniques on uterine scarring.^{12,36} In addition, translational studies might test whether the knowledge gained from animal models can be transferred to human uterine wound healing.^{12–14} Furthermore, we propose that a uterine scar and the unscarred myometrium are not two tissue entities neatly separated from each other. Between the fibrotic LUS and the unscarred myometrium, there might be a transition zone. To date, whether it is actually the fibrotic scar tissue that tears during uterine rupture remains unclear. It could just as well be that the transition area between the scar and the unscarred myometrium represents a predetermined breaking point. We suggest considering this concept in future research projects. At last, further research should be directed to understanding collagen remodelling

of uterine scars during pregnancy, as this might be a potential risk factor or targeting point to prevent uterine rupture. The strength of the study lies in the new LMD-guided approach and the correlation of several techniques to assess uterine scarring.²² Both histological assessments and qPCR yield quantifiable results with significant differences between scarred and unscarred tissues. A limitation is the FFPE tissue that was used for qRT-PCR. Although an established protocol for extracting RNA of adequate quality and quantity from FFPE samples on glass slides was employed,²² downstream molecular applications might be simplified by using fresh frozen samples instead.³⁷ Comparison of collagen density was more than three times higher in the scar area of each sample, but did not reach statistical significance due to small sample size ($p = 0.11$, $n = 3$). It seems reasonable to include more patients in future TEM studies of uterine scars.

5 | CONCLUSIONS

Uterine scars have a significantly higher collagen content in comparison to unscarred myometrium. A high collagen content correlates positively with COL1A2 and COL3A1 gene expression and negatively with the COL1A2/COL3A1 ratio. These quantitative assessments of uterine scars can inform further analyses of specific factors that mediate uterine wound healing.

AUTHOR CONTRIBUTIONS

Alexander Paping: Study design, sample collection, performing caesarean deliveries, sample analyses, data analysis, writing of the manuscript and revision of the manuscript. **Clara Basler:** Sample collection, sample analyses, data analysis and revision of the manuscript. **Loreen Ehrlich:** Study design, sample collection, laboratory analyses, data analysis and revision of the manuscript. **Carlo Fasting:** High-performance liquid chromatography, data analysis and revision of the manuscript. **Kerstin Melchior:** Study design, sample collection, laboratory analyses, data analysis and revision of the manuscript. **Thomas Ziska:** Study design, sample collection, laboratory analyses, data analysis and revision of the manuscript. **Mario Thiele:** Programming of the software plugin for collagen quantification, data analysis and revision of the manuscript. **Georg N. Duda:** study design and revision of the manuscript. **Sara Timm:** Transmission electron microscopy, data analysis and revision of the manuscript. **Matthias Ochs:** study design, transmission electron microscopy, data analysis and revision of the manuscript. **Rebecca C. Rancourt:** Study design, laboratory analyses, data analysis and revision of the manuscript. **Wolfgang Henrich:** Study design, performing caesarean deliveries and revision of the manuscript. **Thorsten Braun:** Study design, sample collection, performing caesarean deliveries, sample analyses, data analysis, revision of the manuscript. All authors reviewed and approved the final submitted version of the manuscript.

ACKNOWLEDGEMENTS

We thank Andrea Stroux from the Institute of Biometry and Clinical Epidemiology at Charité Universitätsmedizin Berlin for statistical counselling. We thank Prof. Dr. Matthias David for his assistance in

enrolling subjects and collecting samples at the Department of Gynaecology, Charité Universitätsmedizin Berlin. We thank Petra Schrade (Core Facility Electron Microscopy, Charité—Universitätsmedizin Berlin) for excellent technical assistance. A linear transducer for intraoperative ultrasound was provided (on loan) for the study by GE Healthcare (Chicago, Illinois, USA). We are also indebted to all the staff of our Department of Obstetrics and Gynaecology and of course the women participants in this study. Open Access funding enabled and organized by Projekt DEAL.

FUNDING INFORMATION

The study was funded by the Deutsche Forschungsgemeinschaft Research Grants Program (grant numbers: SCHW 1946/2-1 and BR 2925/11-1) and by the university research fund of Charité - Universitätsmedizin Berlin (grant number: 51517172-01).

CONFLICT OF INTEREST STATEMENT

The authors report no conflict of interest.

DATA AVAILABILITY STATEMENT

Raw data is available in the data repository figshare at <https://doi.org/10.6084/m9.figshare.22468891>.

ORCID

Alexander Paping  <https://orcid.org/0000-0003-2360-6016>

Matthias Ochs  <https://orcid.org/0000-0002-0936-6979>

Thorsten Braun  <https://orcid.org/0000-0002-1989-9920>

REFERENCES

1. Dimitrova D, Kästner AL, Kästner AN, Paping A, Henrich W, Braun T. Risk factors and outcomes associated with type of uterine rupture. *Arch Gynecol Obstet*. 2022;306(6):1967-1977.
2. Tinelli A, Vergara D, Ma Y, Malvasi A. Dystocia, uterine healing and uterine innervation: an unexplored intersection. *Curr Protein Pept Sci*. 2020;21(5):440-442.
3. Tanos V, Toney ZA. Uterine scar rupture - prediction, prevention, diagnosis, and management. *Best Pract Res Clin Obstet Gynaecol*. 2019;59:115-131.
4. Uchida H, Machida M, Miura T, et al. A xenogeneic-free system generating functional human gut organoids from pluripotent stem cells. *JCI Insight*. 2017;2(1):e86492.
5. Diao J, Liu J, Wang S, et al. Sweat gland organoids contribute to cutaneous wound healing and sweat gland regeneration. *Cell Death Dis*. 2019;10(3):238.
6. Pedroza M, Welschhans RL, Agarwal SK. Targeting of cadherin-11 decreases skin fibrosis in the tight skin-1 mouse model. *PloS One*. 2017;12(11):e0187109.
7. Makino K, Makino T, Stawski L, Lipson KE, Leask A, Trojanowska M. Anti-connective tissue growth factor (CTGF/CCN2) monoclonal antibody attenuates skin fibrosis in mice models of systemic sclerosis. *Arthritis Res Ther*. 2017;19(1):134.
8. Pollio F, Staibano S, Mascolo M, Salvatore G, Persico F, Falco M de, Di Lieto A. Uterine dehiscence in term pregnant patients with one previous cesarean delivery: growth factor immunoexpression and collagen content in the scarred lower uterine segment: growth factor immunoexpression and collagen content in the scarred lower uterine segment. *Am J Obstet Gynecol* 2006;194(2):527-534.

9. Wu C, Chen X, Mei Z, et al. A preliminary study of uterine scar tissue following cesarean section. *J Perinat Med.* 2018;46(4):379-386.
10. Buhimschi CS, Buhimschi IA, Yu C, et al. The effect of dystocia and previous cesarean uterine scar on the tensile properties of the lower uterine segment. *Am J Obstet Gynecol.* 2006;194(3):873-883.
11. Buhimschi CS, Zhao G, Sora N, Madri JA, Buhimschi IA. Myometrial wound healing post-caesarean delivery in the MRL/MpJ mouse model of uterine scarring. *Am J Pathol.* 2010;177(1):197-207.
12. Lapointe-Milot K, Rizcallah E, Takser L, Abdelouhab N, Duvareille C, Pasquier J-C. Closure of the uterine incision with one or two layers after caesarean section: a randomized controlled study in sheep. *J Matern Fetal Neonatal Med.* 2014;27(7):671-676.
13. O'Brien JM, Whetham D, Fecteau C, Jansen J, Hiles M. Augmenting myometrial healing after cesarean delivery: use of an adjuvant biologic graft placement in an ovine model. *Am J Perinatol.* 2011;28(7):543-550.
14. Lin N, Li X, Song T, et al. The effect of collagen-binding vascular endothelial growth factor on the remodeling of scarred rat uterus following full-thickness injury. *Biomaterials.* 2012;33(6):1801-1807.
15. Klinge U, Si ZY, Zheng H, Schumpelick V, Bhardwaj RS, Klosterhalfen B. Collagen I/III and matrix metalloproteinases (MMP) 1 and 13 in the fascia of patients with incisional hernias. *J Invest Surg.* 2001;14(1):47-54.
16. Langenbach MR, Lisovets R, Varga-Szabo D, Bonicke L. Decreased collagen ratio type I/III in association with hemorrhoidal disease. *J Transl Sci.* 2018;5(5):1-4.
17. Manturova NE, Smirnova GO, Stupin VA, Silina EV. The ratio of collagen types I/III as a marker of skin aging and prognosis of aesthetic facial surgery results. *J Pharm Sci Res.* 2018;10(10):2543-2546.
18. Rangaraj A, Harding K, Leaper D. Role of collagen in wound management. *Wounds UK.* 2011;7(2):54-63.
19. Paping A, Basler C, Melchior K, et al. Intraoperative ultrasound during repeat cesarean delivery facilitates sampling of uterine scar tissue. *J Perinat Med.* 2022;51(1):87-96.
20. Schwickerdt A, Henrich W, Vogel M, et al. Placenta Percreta presents with Neoangiogenesis of arteries with Von Willebrand factor-negative endothelium. *Reprod Sci.* 2022;29(4):1136-1144.
21. Tejiram S, Kavalukas SL, Shupp JW, Barbul A. Wound healing. *Wound Healing Biomaterials.* Elsevier; 2016:3-39.
22. Paping A, Basler C, Rancourt R, et al. Optimized RNA isolation of FFPE uterine scar tissues for RNA expression analyses delineated by laser microdissection. *Biotechniques.* 2022;72(6):273-278.
23. Arrowsmith S. Identification and validation of suitable reference genes for quantitative real-time PCR gene expression analysis in pregnant human myometrium. *Mol Biol Rep.* 2021;48(1):413-423.
24. Edwards CA, O'Brien WD. Modified assay for determination of hydroxyproline in a tissue hydrolyzate. *Clin Chim Acta.* 1980;104(2):161-167.
25. Monticelli E, Aman CS, Costa ML, et al. Simultaneous free and glycosylated pyridinium crosslink determination in urine: validation of an HPLC-fluorescence method using a deoxypyridinoline homologue as internal standard. *J Chromatogr B Analyt Technol Biomed Life Sci.* 2011;879(26):2764-2771.
26. Reynolds ES. The use of lead citrate at high pH as an electron-opaque stain in electron microscopy. *J Cell Biol.* 1963;17(1):208-212.
27. Tschanz S, Schneider JP, Knudsen L. Design-based stereology: planning, volumetry and sampling are crucial steps for a successful study. *Ann Anat.* 2014;196(1):3-11.
28. Gundersen HJG. Notes on the estimation of the numerical density of arbitrary profiles: the edge effect. *J Microsc.* 1977;111(2):219-223.
29. Edwards LK. In: Dekker M, ed. *Applied Analysis of Variance in Behavioral Science.* Marcel Dekker; 1993:297-344.
30. Sevket O, Ates S, Molla T, Ozkal F, Uysal O, Dansuk R. Hydrosonographic assessment of the effects of 2 different suturing techniques on healing of the uterine scar after cesarean delivery. *Int J Gynaecol Obstet.* 2014;125(3):219-222.
31. McKleroy W, Lee T-H, Atabay K. Always cleave up your mess: targeting collagen degradation to treat tissue fibrosis. *Am J Physiol Lung Cell Mol Physiol.* 2013;304(11):L709-L721.
32. Nissen R, Cardinale GJ, Udenfriend S. Increased turnover of arterial collagen in hypertensive rats. *Proc Natl Acad Sci U S A.* 1978;75(1):451-453.
33. Bashey RI, Cox R, McCann J, Jimenez SA. Changes in collagen biosynthesis, types, and mechanics of aorta in hypertensive rats. *J Lab Clin Med.* 1989;113(5):604-611.
34. Mathew-Steiner SS, Roy S, Sen CK. Collagen in wound healing. *Bioengineering (Basel).* 2021;8(5):63.
35. Lofrumento DD, Di Nardo MA, de Falco M, Di Lieto A. Uterine wound healing: a complex process mediated by proteins and peptides. *Curr Protein Pept Sci.* 2017;18(2):125-128.
36. Kaps C, Schwickerdt A, Dimitrova D, et al. Online survey on uterotomy closure techniques in caesarean section. *J Perinat Med.* 2021;49(7):809-817.
37. Chung J-Y, Braunschweig T, Williams R, et al. Factors in tissue handling and processing that impact RNA obtained from formalin-fixed, paraffin-embedded tissue. *J Histochem Cytochem.* 2008;56(11):1033-1042.

SUPPORTING INFORMATION

Additional supporting information can be found online in the Supporting Information section at the end of this article.

How to cite this article: Paping A, Basler C, Ehrlich L, et al. Uterine scars after caesarean delivery: From histology to the molecular and ultrastructural level. *Wound Rep Reg.* 2023; 31(6):752-763. doi:[10.1111/wrr.13127](https://doi.org/10.1111/wrr.13127)